

CORONAL MAGNETIC FIELD MEASUREMENTS

H. LIN, J. R. KUHN, AND R. COULTER

Institute for Astronomy, University of Hawaii, 2680 Woodlawn Drive, Honolulu, HI 96822

Received 2004 June 28; accepted 2004 August 19; published 2004 August 31

ABSTRACT

A long-standing solar problem has been to measure the coronal magnetic field. We believe it determines the coronal structure and dynamics from the upper chromosphere out into the heliospheric environment. It is only recently that Zeeman splitting observations of infrared coronal emission lines have been successfully used to deduce the coronal magnetic flux density. Here we extend this technique and report first results from a novel coronal magnetometer that uses an off-axis reflecting coronagraph and optical fiber-bundle imaging spectropolarimeter. We determine the line-of-sight magnetic flux density and transverse field orientation in a two-dimensional map with a sensitivity of about 1 G with 20" spatial resolution after 70 minutes of integration. These full-Stokes spectropolarimetric measurements of the forbidden Fe XIII 1075 nm coronal emission line reveal the line-of-sight coronal magnetic field 100" above an active region to have a flux density of about 4 G.

Subject headings: instrumentation: polarimeters — magnetic fields — Sun: corona

1. INTRODUCTION

The coronal magnetic field is something of a “dark energy” problem for us in that we know it permeates the corona and controls its static and dynamic behavior, yet we are unable to usefully measure it. Obtaining the magnetic field along even a single coronal line of sight is a difficult observational problem. There have been a few measurements of the coronal magnetic field along sight lines to radio sources that allow for Faraday rotation measurements (Patzold et al. 1987) or from the Faraday rotation of polarized solar radiation (Alissandrakis & Drago 1995). It is also possible that radio gyrosynchrotron magnetometry techniques will become generally useful for inferring active region field strengths low in the corona (e.g., Gary & Hurford 1994), but these techniques are still developing. Here we demonstrate significant progress toward this goal using sensitive imaging spectropolarimetric observations of the infrared forbidden coronal emission line (CEL) of Fe XIII at a wavelength of 1075 nm relatively high in the corona.

It has been known since the first quantitative observations of the IR CELs of Fe XIII at 1075 and 1080 nm by Firor & Zirin (1962) that these lines have important diagnostic potential for determining physical conditions of the coronal plasma near a temperature of 2 MK. Chevalier & Lambert (1969) and Flower & Pineau des Forêts (1973) described the exquisite sensitivity of the IR Fe XIII lines to the local electron density. Harvey (1969) was one of the first to attempt Stokes V (using Fe XIV at 530 nm) measurements to search for magnetic fields. Mickey (1973) successfully used this line to measure the coronal B -field direction. Somewhat later, House (1977) showed with detailed line formation calculations, and Querfeld (1977) with observations, how the linear polarization of the 1075 nm line was quite sensitive to the coronal magnetic field orientation.

Armed with a modern IR array detector, Kuhn (1995) looked for Stokes V (circular) polarization of Fe XIII 1075 nm and argued that such IR Zeeman splitting observations could, in principle, achieve coronal magnetic flux density sensitivities of a few gauss. Judge (1998) carefully modeled the Fe XIII lines' Zeeman sensitivity and quantified their magnetometry potential. This is a difficult polarization measurement requiring relative photometric sensitivity at the level of 10^{-4} in order to recover the coronal magnetic flux density with an accuracy of

a few gauss. It was Lin et al. (2000) who first convincingly demonstrated this. Their measurement along a single sight line above an active region revealed a flux density of about 30 G. The observations took advantage of the strong IR Fe XIII CEL at 1075 nm with a sensitive IR array detector and spectropolarimeter. Except for a recent effort by the High Altitude Observatory group (Tomczyk et al. 2004), we are not aware of other attempts at coronal Zeeman magnetometry. Here we describe the first two-dimensional coronal magnetic field map as it was enabled by a new optical fiber-bundle imaging spectropolarimeter (OFIS).

2. THE SOLARC CORONAGRAPH AND OFIS

The Solar Observatory for Limb Active Regions and Coronalae (SOLARC) is a 0.46 m off-axis (unobscured) reflecting coronagraph at the summit of Haleakala on Maui. It combines a large aperture (by present solar telescope standards) with a fully achromatic, low scattered light optical design and was built to demonstrate and explore coronal Zeeman magnetometry (Kuhn et al. 2003).

SOLARC has a relatively fast focal ratio and is particularly well suited for low spatial resolution faint coronal spectropolarimetry. The Gregorian focus OFIS consists of a tunable liquid crystal variable retarder and a 16×8 coherent fiber bundle and lenslet array (H. Lin, R. Coulter, & J. R. Kuhn 2004, in preparation). Each 125 μm fiber subtends approximately 20" in a rectangular pattern $5' \times 2'.5$. The 25 m long coherent bundle generates 128 distinct spectra at the spectrograph image plane on a bench-mounted conventional Ebert-Fastie spectrograph. It uses a 79 line mm^{-1} echelle grating and yields a dispersion of 0.017 nm pixel^{-1} on our Rockwell NICMOS HgCdTe 256×256 array detector. With OFIS, we can measure the full Stokes (I , Q , U , V) linear and circular polarized intensity in the near-IR (1–2.5 μm) spectrum.

3. NEAR-INFRARED CORONAL SPECTROPOLARIMETRY

The corona was observed on 2004 April 6 near the west limb passage of NOAA Active Region 581. The OFIS field of view for Stokes V polarimetry extended from about 0.1 to 0.45 R_{\odot} from the west limb and was obtained from 70 minutes of integration time during a 3 hr period. Four other shorter off-pointed

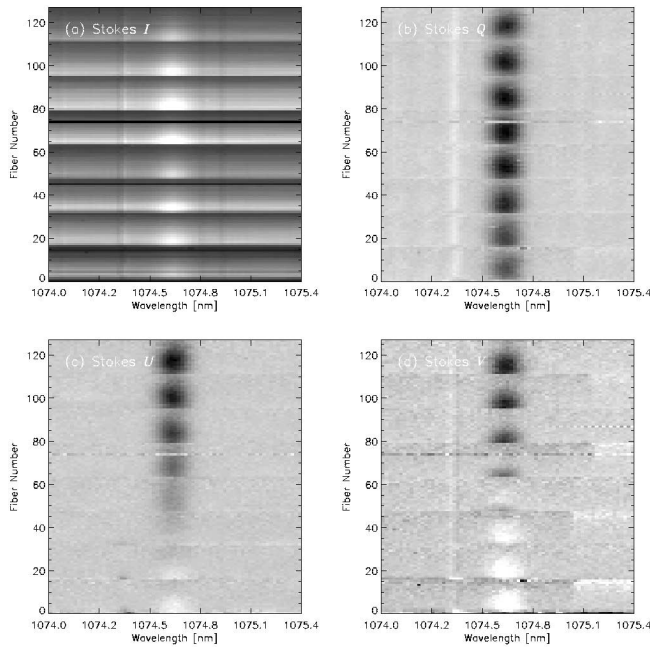


FIG. 1.—Stokes I , Q , U , V spectra are shown for each of 128 fiber positions. The display range is $\pm 50\%$ for I , $\pm 5\%$ for Q and U , and $\pm 0.5\%$ for V (each normalized by the 20 millionths of disk brightness mean continuum intensity). Each group of 16 fibers corresponds to one east-west row, with the bottom group corresponding to the southernmost row. This field of view was near NOAA AR 581 as it passed near the west solar limb.

observations of the surrounding coronal region were also obtained to measure linear polarization.

Figure 1 shows a gray-scale image rendition of the spectropolarimetric data from each of the 128 fibers. The dispersion runs horizontally, and each row of the image shows the spectrum of a distinct spatial region in the corona. Successive groups of 16 spectra come from a single row in the 16×8 bundle. Thus, the fibers closest to the limb (easternmost) are brightest within each group of 16. The bottom 16-spectra group in each panel of the figure corresponds to the 16-fiber row farthest south in the fiber bundle.

The Stokes I spectra were flat-fielded by a “sky flat” taken at $1.75 R_{\odot}$ above the limb. Weak atmospheric absorption lines persist in this flat field and can be seen in the spectra in Figure 1a. The scattered light Fraunhofer line of Si I near 1074.3 nm appears as a dark-light doublet because the scattered light flat field and coronal regions have slightly different Si I Doppler velocities. The bright Fe XIII emission line near 1074.7 nm is unaffected by flat-field line contamination because there are no photospheric lines in this region. The two faint dark lines near 1074.8 and 1074.9 nm are telluric absorption lines and are unshifted between the coronal and flat-field telescope pointings.

Figures 1b and 1c show the Stokes Q and U data obtained from the difference of orthogonal linear polarized spectra. Note that the scattered Si I light is weakly linearly polarized, independent of field position (fiber), while the CEL shows a large variable linear polarization direction, as expected, owing to the sensitivity of the CELs’ linear polarization sensitivity to the magnetic direction. The polarization of the forbidden CELs is described by the resonant scattering polarization in the “effectively strong field” regime (House 1974), which is sometimes referred to as the “saturated” Hanle effect when the Larmor frequency is much larger than the spontaneous line transition

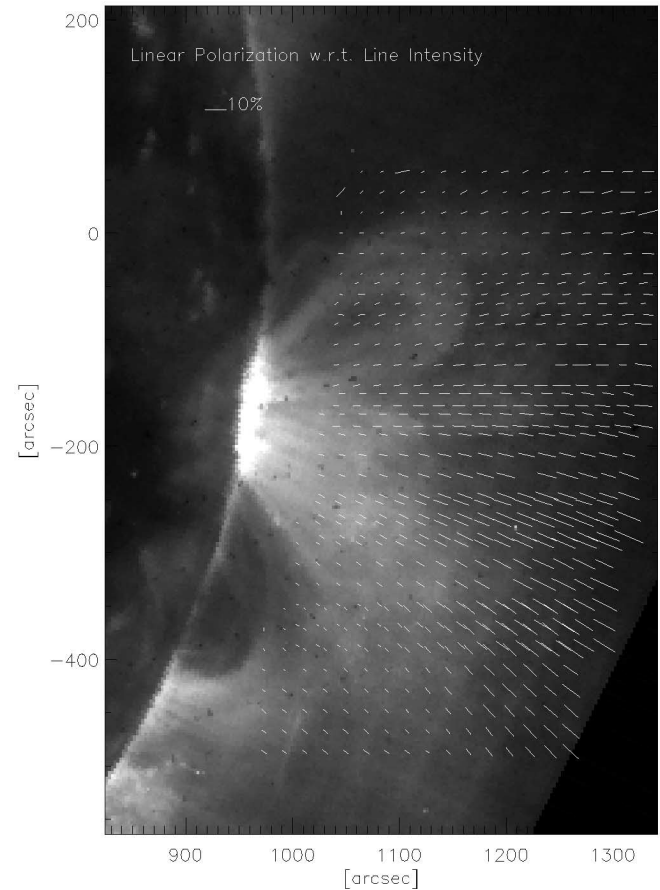


FIG. 2.—Measured linear polarization of Fe XIII for all of the pointings near NOAA AR 581, superposed on an EIT 28.4 nm Fe XV image. The plotted lines show the magnitude and direction of the linear polarization. The overlapping telescope pointings and fiber positions cause the nonuniform spatial sampling.

rates. In this case, only the polarization direction is a function of the direction of the magnetic field. The Q , U gray-scale plots and all our Stokes polarization data are normalized by the nearby scattered light continuum intensity level of approximately 20 millionths of the disk center intensity. The dark to light intensity scale is plotted here for Q and U with a $\pm 5\%$ polarization range.

Figure 1d shows the derived Stokes V spectra obtained from the difference of orthogonal circular polarizations, normalized by the mean continuum intensity (detector flat fields have not been applied to the Stokes Q , U , and V data). The display range here is much smaller— $\pm 0.5\%$. It is notable that the scattered photospheric Si I light shows a light-dark doublet characteristic of an “antisymmetric” V -line profile. This is due to the photospheric Stokes V signal caused by the nonzero mean line-of-sight solar disk magnetic field. In contrast, the Fe XIII line shows a wavelength dependence to the V -line profile that is superficially similar to the Stokes I , Q , and U profiles rather than being antisymmetric in wavelength. This is a consequence of the large linear polarization of the CEL and the small, but significant, observational cross talk between Stokes Q/U and V polarization. This effect must be calibrated and removed in order to measure the coronal B field.

Figure 2 shows the direction and linear polarization magnitude obtained from each of the pointings near NOAA AR 581. These results are qualitatively similar to comparable res-

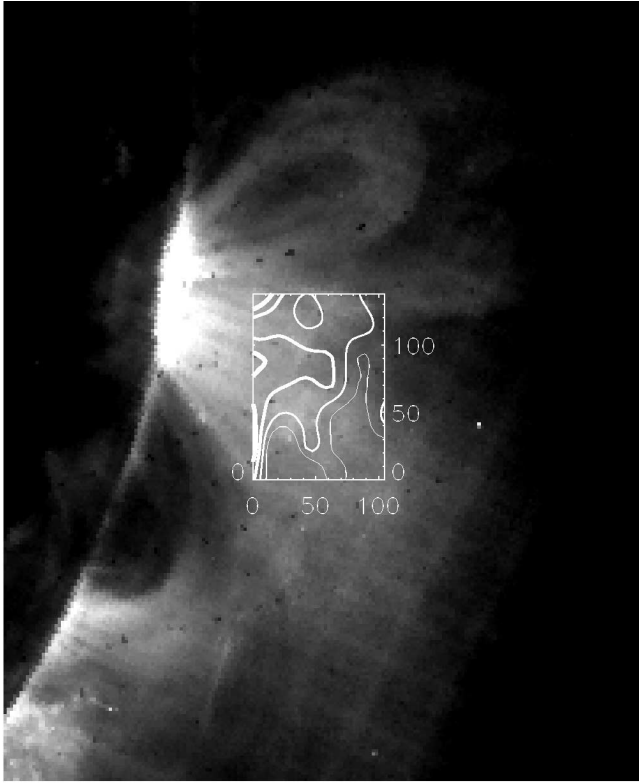


FIG. 3.—Contour map (based on $20''$ pixels) of the measured coronal magnetic field strength using Fe XIII overlaid on the EIT Fe XV image. The thick contour corresponds to 4 G, with additional contours corresponding to flux densities of 2, 0, and -2 G. Tick marks indicate the spatial scale in units of arcseconds.

olution Fe XIII linear polarimetry obtained during eclipse conditions (Habbal et al. 2003). Our data are superposed over an EUV Imaging Telescope (EIT) 28.4 nm Fe XV image. We might expect the polarization to trace the local coronal magnetic field since it is this magnetized plasma that scatters photospheric light. This expectation is weakened by the Van Vleck effect (cf. House 1974; Lin & Casini 2000; Casini 2002), which rotates the polarization perpendicular to the field when the angle between the local B field at the scattering center and the local solar radial direction are larger than the Van Vleck angle (about 55°). When this angle is close to the Van Vleck angle, the polarization amplitude approaches zero. Certainly the tops of loops should exhibit polarization perpendicular to the projected field direction while other parts of a loop should scatter polarized light with a varying but generally nonradial polarization that follows the loop. We see from Figure 2 that the observed polarization does tend to “respond” to the underlying loop structure, although it is also clear that this tendency is more complicated than the simple correspondence implied if the visible loops are a fair tracer of the dominant local magnetic field direction. Note that the degree of linear polarization generally increases away from the limb as the incident scattering radiation becomes more anisotropic and as collisional excitation becomes less important with declining coronal electron density. Further study and more data are needed to fully interpret the Stokes Q and U Fe XIII polarimetry.

3.1. Stokes V Spectropolarimetry

Recovering the coronal Stokes V polarization requires using the independent and simultaneous measurements of intensity

and linear polarization. In the corona, the Zeeman splitting is always small compared to the thermal line broadening so the expected V signal is $V = kB dI/d\lambda$, where I is the line intensity, B is the magnetic field strength in units of gauss, and $k = 6.5 \times 10^{-6} \text{ nm G}^{-1}$ for this Fe XIII line with a Landé factor of 1.5. Here we ignore a correction factor to the standard magnetograph formula for CELs described by Casini & Judge (2000). The observed V' profile is

$$\begin{aligned} V'(\lambda) &= V(\lambda) + \alpha I(\lambda) = kB dI(\lambda)/d\lambda + \alpha I(\lambda) \\ &\approx \alpha I(\lambda + kB/\alpha), \end{aligned}$$

where $\alpha I(\lambda) = M_{IV}I(\lambda) + M_{QV}Q(\lambda) + M_{UV}U(\lambda)$ is the total cross talk between linear and circular polarization at each field point. Unlike a typical photospheric magnetogram, here the large linear CEL polarization and cross talk term dominates the observed circular polarization signal. We make the physically reasonable assumption that $Q(\lambda)$ and $U(\lambda)$ are proportional to $I(\lambda)$. Expressed in this form, it is evident that the effects of the dominant $I - V$, $U - V$, and $Q - V$ cross talk terms are to shift the apparent peak of the V' spectra in wavelength away from the peak of the unpolarized spectrum, $I(\lambda)$. We find that this shift is small but easily measurable with a typical magnitude of a tenth of a pixel in our data.

Since polarized and unpolarized spectra are obtained through identical OFIS optics without optomechanical change, it is straightforward to derive B by least-squares fitting $I(\lambda)$ and $dI/d\lambda$ to the observed V' spectra. To minimize the numerical noise in the derivative, we fit a Gaussian to $I(\lambda)$ and then evaluate the derivative analytically and separately for each fiber. The magnetic field is obtained from the least-squares fitted coefficient of the derivative term. In this way, the array of fibers yields a contour map of the longitudinal coronal field, which is overlaid on the EIT 28.4 nm image in Figure 3. The B field derived from individual fibers (or pixels) is statistically significant in the first four columns closest to the limb.

Since I , Q , and U vary significantly across the field, and the I to V' correlation is directly measured from our fitting procedure, we can derive the polarimetric cross talk, M_{IV} , M_{QV} , and M_{UV} , by correlating this term against the observed I , Q , and U polarization derived for each fiber. Here we assume (as our polarized ray-trace optical modeling justifies) that the $I - U$ and $I - Q$ polarization is small (less than 1% for SOLARC optics) and has insignificant variation across our field. We find that $M_{IV} = -0.0027 \pm 0.0004$, $M_{QV} = -0.094 \pm 0.007$, and $M_{UV} = 0.16 \pm 0.006$. These values may result from the aluminum oxide mirror coating spatial nonuniformity or from non-ideal polarimeter tuning. It is interesting that small residual polarization can be measured using empirical calibration techniques, even when the optical system’s nonideal Mueller matrix terms are of order 10%.

4. DISCUSSION

At a height of $0.1 R_\odot$ in the corona, the field is only a few gauss, but we can still measure statistically significant variations across the OFIS field of view. For example, Figure 4 shows the mean coronal field versus limb distance along with a summary of two theoretical models of the expected coronal field above a “typical” active region. While the models (Abbet & Fisher 2003; S. Ledvina 2004, in preparation) were used for qualitative comparison to gauge the scale and range of expected field strengths, the quantitative agreement suggests that the modeling efforts are realistic. The measured field here is the

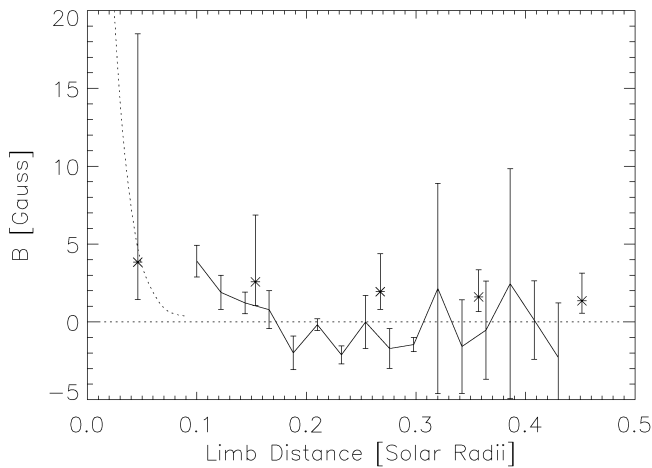


FIG. 4.—The dotted line shows the vertical variation in the rms magnetic field above a 1 kG longitudinal field active region from Abbett & Fisher (2003). The asterisks show the rms field from a global coronal field calculation by S. Ledvina (2004, in preparation). Upper error bars on these points indicate the maximum field strength at this height, and lower error bars show the rms fluctuation in B . The solid curve shows the average measured field from the central 4 pixels in each north-south column. The measured error bars are also indicated.

weighted average of the central 4 pixels from each north-south column of fibers. Note also that the observed coronal field changes sign about 0.15 radii above the limb—perhaps because we are beginning to see through a loop oriented in a plane parallel to our sight line. The mean least-squares fits to cross talk-corrected apparent V profiles are illustrated for each height above the limb in Figure 5.

Measurements like these may finally allow us to understand why some coronal field lines are “lit up” while others are not. For example, is it regions of strongest magnetic field that are brightest? We have looked at the magnitude of the observed field versus the Fe XIII line brightness for those fibers with a statistically significant measured field strength. The correlation coefficient is consistent with zero. This lack of correlation is striking and underscores the fact that we do not understand why and how only some of the space filling the coronal mag-

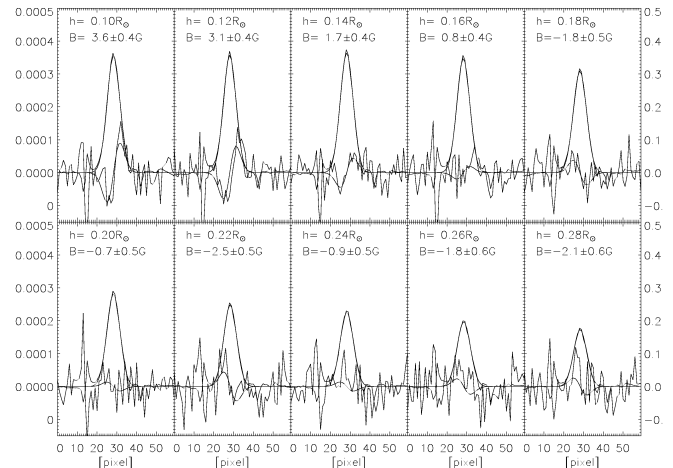


FIG. 5.—Fitted Stokes V profiles and data corrected for Q/U cross talk for the mean of the central 4 pixels in each of the 10 fiber bundle columns closest to the west solar limb. Observed and fitted Stokes I profiles are overplotted and correspond to the scale on the right.

netic field is illuminated by sometimes hot and bright coronal plasma.

The SOLARC/OFIS instrument has produced a useful coronal magnetogram. To improve on this relatively coarse spatial and temporal resolution requires a significantly larger solar coronagraph. We believe that the coronal magnetic studies allowed by such an instrument are likely to be some of the most exciting new opportunities that the Advanced Technology Solar Telescope (Keil et al. 2003) will realize.

This research was supported by the NASA Suborbital Research and Technology program, the Air Force Multidisciplinary University Research Program, the National Science Foundation Stellar Astronomy and Astrophysics and Atmospheric programs, and a Defense University Research Instrumentation Program grant. We are grateful to Don Mickey for helpful comments and to Bill Abbett and Steve Ledvina for providing unpublished results from their coronal models. The National Solar Observatory contributed to the OFIS instrument construction.

REFERENCES

- Abbett, W. P., & Fisher, G. H. 2003, *ApJ*, 582, 475
 Alissandrakis, C. A., & Drago, F. C. 1995, *Sol. Phys.*, 160, 171
 Casini, R. 2002, *ApJ*, 568, 1056
 Casini, R., & Judge, P. 2000, *ApJ*, 533, 574
 Chevalier, R. A., & Lambert, D. L. 1969, *Sol. Phys.*, 10, 115
 Firor, J. W., & Zirin, H. 1962, *ApJ*, 135, 122
 Flower, D. R., & Pineau des Forêts, G. 1973, *A&A*, 24, 181
 Gary, D. E., & Hurford, G. J. 1994, *ApJ*, 420, 903
 Habbal, S. R., et al. 2003, *ApJ*, 592, L87
 Harvey, J. W. 1969, Ph.D. thesis, Univ. Colorado
 House, L. L. 1974, *PASP*, 86, 490
 ———. 1977, *ApJ*, 214, 632
 Judge, P. G. 1998, *ApJ*, 500, 1009
 Keil, S., et al. 2003, *Proc. SPIE*, 4853, 240
 Kuhn, J. R. 1995, in *Infrared Tools for Solar Astrophysics: What's Next?*, ed. J. R. Kuhn & M. J. Penn (Singapore: World Scientific), 89
 Kuhn, J. R., Coulter, R., Lin, H., & Mickey, D. 2003, *Proc. SPIE*, 4853, 318
 Lin, H., & Casini, R. 2000, *ApJ*, 542, 528
 Lin, H., Penn, M., & Tomczyk, S. 2000, *ApJ*, 541, L83
 Mickey, D. L. 1973, *ApJ*, 181, L19
 Patzold, M., et al. 1987, *Sol. Phys.*, 109, 91
 Querfeld, C. W. 1977, *Proc. SPIE*, 112, 200
 Tomczyk, S., et al. 2004, *AAS Meeting*, 204, 20.02